

## Highly Porous Bi(III) Modified Rice Husk Silica Photocatalyst for the Photocatalytic Removal of Cationic Methylene Blue

Normawati Jasni<sup>a</sup>, Anwar Iqbal<sup>a\*</sup>, N. H. H. Abu Bakar<sup>a</sup>, Dede Heri Yuli Yanto<sup>b</sup>, Hor Jia Yi<sup>a</sup>, Noor Haida Mohd Kaus<sup>a</sup>, Mohd Norazmi Ahmad<sup>c</sup>, Sri Mulijani<sup>d</sup>

*a) School of Chemical Sciences, Universiti Sains Malaysia, 11800 USM, Penang, Malaysia*

*b) Research Center for Applied Microbiology, National Research and Innovation Agency (BRIN), Cibinong, Bogor 16911, Indonesia*

*c) Experimental and Theoretical Research Lab, Department of Chemistry, Kulliyah of Science, International Islamic University Malaysia, Bandar Indera Mahkota, 25200 Kuantan, Pahang, Malaysia*

*d) Department of Chemistry, Bogor Agriculture University-Bogor-Indonesia, Indonesia*

Received 31 July 2023; received in revised form 14 September 2023; accepted 23 September 2023 (DOI: 10.30495/IJC.2023.1992759.2033)

### ABSTRACT

A series of bismuth-silicate photocatalysts were synthesized via the sol-gel method for photodegradation of methylene blue (MB) under sunlight irradiation, utilizing rice husk ash as a silica precursor. The scanning electron microscopy/energy dispersive X-ray (SEM/EDX) analysis detected Bi content in 3-10 wt% range. Furthermore, it can be seen that the porosity decreased as the Bi concentration increased. The N<sub>2</sub> adsorption-desorption analysis indicates the presence of mesopores with an average diameter of 297-554 Å with Brunauer–Emmett–Teller (BET) surface area of 5.6-30.5 m<sup>2</sup>/g. The photocatalyst with a Bi concentration of 4 wt% (RHSBi-A2) was the most active in the photodegradation of MB; the removal reached 90% within 4 h. The photodegradation is proposed to be driven by superoxide (O<sub>2</sub><sup>-</sup>), hydroxyl (•OH) radicals, and hole (h<sup>+</sup>) based on the valence band (VB) and conduction band (CB) potentials. The porous silica framework is proposed to act as an electron reservoir, allowing better MB adsorption and enhancing light absorption.

**Keywords:** Bismuth, Mesoporous silica, Methylene blue, Photocatalyst, Rice husk, Sunlight

### 1. Introduction

The textile industry is a multi-million-dollar business that has improved the lives of millions of people around the world. Regardless, the wastewater contaminated with dyes released to the water bodies without proper treatment may lead to environmental and humanitarian problems. Once in water bodies in large quantities, these dyes can prevent the sunlight from penetrating the surface, inhibiting the ability of aquatic plants to carry on photosynthesis and lowering the dissolved oxygen content, eventually creating an anoxic environment [1–3]. The World Bank has identified 72 toxic chemicals originating solely from textile dyeing [4].

Methylene blue (methylthionium chloride, MB) is a popular cationic dye used in coloring cotton, silk produ-

-cts, temporary hair colours, pigments, paints, and papers [5, 6]. The MB has a complex aromatic structure, making the dye resistant to heat and light. Hence, MB does not decompose in water under natural conditions, and the biodegradation of this dye is a very long process [7]. When the MB enters the human body, it damages the neurological system [8, 9]. In addition, it is also known as a potent carcinogen for several marine creatures [8]. Hence, MB is categorized as poisonous, carcinogenic, and non-biodegradable [10].

The phenolic and aromatic components of the dye molecular structure inhibit the ability of conventional wastewater systems to remove them [11, 12]. Methods such as flocculation, coagulation, membrane separation, and adsorption have drawbacks, such as post-remediation due to sludge production and adsorbent

\*Corresponding author:

E-mail address: [anwariqbal@usm.my](mailto:anwariqbal@usm.my) (A. Iqbal)

removal [13]. Photocatalysis using photocatalysts is a promising method to degrade the phenolic and aromatic components of the dye effectively. When a photocatalyst absorbs photons equal to or greater than its band gap, electrons ( $e^-$ ) will be excited from the valence band (VB) to the conductive band (CB), leaving behind holes ( $h^+$ ) in the VB. The photogenerated  $e^-/h^+$  pairs diffuse to the surface, oxidising and reducing oxygen and water molecules to reactive radicals such as superoxide ( $O_2^{\cdot-}$ ) or hydroxyl ( $OH^{\cdot}$ ) radicals. These radicals can mineralise the organic pollutants into carbon dioxide ( $CO_2$ ) and water ( $H_2O$ ) [14, 15]. Regardless, photocatalysts suffer from several drawbacks, such as photo corrosion, low light sensitivity due to wide band gap, rapid recombination of photogenerated  $e^-/h^+$  pairs, low surface area, rapid deactivation, and agglomeration [16].

The separation of photogenerated  $e^-/h^+$  pairs must be prolonged to ensure maximum production of radicals. The maximum separation can be achieved through several approaches. (i) The distance for the pairs to reach the surface to generate the radicals for photocatalysis before recombining can be suppressed by reducing the size of the photocatalyst. (ii) Doping with metals and non-metals can create novel/mixed energy levels or form heterojunctions. These energy levels act as traps, whereas the heterojunctions provide alternative flow pathways to keep the photogenerated  $e^-$  away from the  $h^+$ . In addition, doping can narrow the band gap to enhance the absorption of photons over broader electromagnetic radiation. The photogenerated pairs can also be kept separated through plasmonic systems by incorporating metallic nanoparticles, such as Au, Ag, or Cu. These metals exhibit the surface plasmon resonance (SPR) effect, which can convert visible light to chemical energy and separate the photogenerated  $e^-/h^+$  pairs produced on the surface of the semiconductor. Immobilizing the photocatalysts on porous support increases the surface area, prevents agglomeration, and allows better light absorption [17, 18].

Bismuth-silicate photocatalysts are a fascinating class of nanocomposites with unique functionalities, cleaner production, and sustainability due to their large specific surface area, size, and morphology [19]. Adding bismuth, even in a small quantity, can cause significant changes in silica's properties. Mohamed et al. [20] and Belik et al. [19] reported that adding Bi reduced the adsorption of MB on the surface of the photocatalyst. Hence, this allows more photons to reach the surface of the photocatalysts, creating an enhanced photocatalysis process. El-Hakam et al. [21], on the other hand, reported that mesoporous silica improved the photocatalytic ability of  $BiVO_4$  in removing MB and

brilliant green (BG) dyes under visible light by suppressing the recombination rate of photogenerated  $e^-/h^+$  pairs. The removal of MB and BG was determined to be 90.8% and 80.9%, respectively, after 60 min. Anthony et al. [3] synthesised silica-modified self-assembled bismutite (BSC) structures through a facile hydrothermal route. The presence of silica has improved MB's adsorption properties due to silanol groups, which could form hydrogen bonding and enhance the electrostatic interaction. As a result of good adsorption, faster mineralization of MB was achieved. The total organic carbon (TOC) analysis indicated 20 % better mineralization.

Silica precursors frequently used in the synthesis of siliceous nanocomposites, such as tetraethyl orthosilicate (TEOS), tetramethyl ortosilicate (TMOS), sodium silicate, etc., are of synthetic origin. They are produced through chemical processes that require harsh conditions and reagents, high cost, and generates huge volumes of effluents [22, 23]. Rice (*Oryza sativa*) can take up to 230-470 kg  $ha^{-1}$  of Si from soil to maintain its healthy growth. Rice husks and rice husk ash contain high-purity amorphous silica that can be used as an alternative source to replace silica precursors from synthetic origins. The silica can be extracted from rice husk and rice husk ash through several methods such as solvent extraction and pyrolysis [24,25]. These methods consume less energy and chemicals than conventional silica synthesis.

Herein, we report the synthesis of bismuth-silicate nanocomposite photocatalysts utilizing rice husk ash as silica precursor via the sol-gel method for the photodegradation of MB under sunlight. The synthesized photocatalysts were characterised using various microscopic and spectroscopic analyses, such as X-ray diffraction (XRD),  $N_2$  adsorption-desorption, UV-Visible spectrophotometry diffuse reflectance spectroscopy (UV-Vis DRS), Scanning electron microscopy/energy dispersive X-ray (SEM/EDX), Raman spectroscopy and Fourier transform infrared (FT-IR) spectroscopy to understand its physicochemical properties. Parameters studied in the photodegradation of MB were the effect of pH, the effect of bismuth concentration, the effect of MB initial concentration, and photocatalyst dosage. This work highlights the use of agricultural biomass, rice husk as silica precursor for the synthesis of highly porous bismuth-silicate photocatalysts via the sol-gel method without the need for excessive chemical use and harsh reaction conditions for MB removal. The outcome of this work also contributes to the fulfillment of United Nations Sustainable Development Goals (SDGs) 6, clean water and sanitary.

## 2. Experimental

### 2.1. Chemicals and Materials

Bismuth(III) nitrate pentahydrate ( $\text{Bi}(\text{NO}_3)_3 \cdot 5\text{H}_2\text{O}$ , ACS reagent,  $\geq 98\%$ ), sodium hydroxide pellets (Qrec), nitric acid (System, 65%) and MB were used as received without further purification. Rice husk was collected from a rice mill in Penang, Malaysia.

### 2.2. Preparation of rice husk ash silica

The rice husk ash silica preparation method was adopted by Adam and Iqbal [26]. The rice husk was first washed with tap water to remove dust and dirt and dried in an oven at 373 K for 2 h. The dried rice husk (30 g) was then treated with 1 L of 1.0 M nitric acid ( $\text{HNO}_3$ ) for 24 h. The acid-treated rice husk was washed with distilled water until clear decanted water with constant pH was obtained. The samples were then oven-dried at 373 K for 24 h before being subjected to calcination at 873 K for 6 h to obtain white rice husk ash silica (RHS).

### 2.3. Sol-gel synthesis of bismuth-silicate (RHSBi) photocatalysts

The synthesis of RHSBi photocatalysts was adopted from Yi Yao et al. [27] with some modifications. A 3.00 g of RHS was added into 100 mL of 0.8 M sodium hydroxide solution (NaOH). The RHS was dissolved at 353 K under continuous stirring for 1 h. The resulting sodium silicate solution was filtered to obtain a clear filtrate. Bismuth nitrate solution was separately prepared by dissolving 0.17 g, 0.35 g, 0.52 g, or 0.70 g (based on silica weight) of  $\text{Bi}(\text{NO}_3)_3 \cdot 5\text{H}_2\text{O}$  in 20 mL of 2.0 M of  $\text{HNO}_3$  at 303 K. The  $\text{Bi}(\text{NO}_3)_3 \cdot 5\text{H}_2\text{O}$  solution was then titrated into sodium silicate solution at a 0.5 mL/min rate. The titration was continued using 2.0 M  $\text{HNO}_3$  until pH 10 to produce precursor gel. The gel was aged for 24 hours under stirring. The product was separated from its precursor mixture *via* centrifugation. The residue was filtered and rinsed with hot distilled water to remove any physically adsorbed bismuth oxides. The product was dried in the oven at 373 K for 24 h. The dried product was ground into a fine powder and calcinated at 823 K for 6 h. The prepared catalysts were labeled as RHSBi-A1, RHSBi-A2, RHSBi-A3 and RHSBi-A4.

### 2.4. Catalyst characterisation

The structural properties of RHS and RHSBi photocatalysts were characterized using X-ray diffraction (XRD) analysis (Cu  $K\alpha$  radiation,  $\lambda=1.54060$

Å,  $2\theta=10-90^\circ$ ). The porosity of the resulting catalysts was determined with  $\text{N}_2$  adsorption-desorption analysis, while their textures and morphologies were observed with a scanning electron microscope (SEM). Energy dispersive spectrometry (EDX) was employed to measure the bismuth concentration. The UV-Visible spectrophotometry diffuse reflectance spectroscopy (Uv-Vis DRS) was performed with a Perkin Elmer Lambda 35 UV-Vis spectrophotometer using  $\text{BaSO}_4$  as a reference to determine the absorption wavelength and band gap. Raman spectroscopy and Fourier Transform infrared spectroscopy (FTIR, Perkin Elmer System 2000, 400-4000  $\text{cm}^{-1}$ , 100 scans, KBr disc method) were used to identify the functional groups.

### 2.5. Determination of pH of point of zero charges

The RHSBi photocatalysts' pH of point of zero charges ( $\text{pH}_{\text{PZC}}$ ) was determined using the salt addition method based on the method reported by Divband et al. [28] with some modifications. As many as 5 portions of sodium nitrate (20 mL, 1.0 M) were prepared in a beaker. The pH of the solutions was adjusted to pH 3, 5, 7, 7.5, 8.5, 9, and 11 by using 0.01 M HCl and 0.01M NaOH solution. As much as 25 mg of the photocatalysts were added into the solution and the initial pH was recorded. The beakers were covered with parafilm and shaken in the dark for 24 h at 250 rpm using a shaker to attain equilibrium. The  $\Delta\text{pH}$  is calculated after 24 h and plotted against the initial pH of the solution. The  $\text{pH}_{\text{PZC}}$  is determined at the pH where the  $\Delta\text{pH} = 0$ .

### 2.6. Photodegradation of methylene blue (MB)

Methylene blue concentrations of 10 ppm, 15 ppm, 20 ppm, and 25 ppm were prepared by diluting 100 ppm stock solution. A specific amount of photocatalyst was added to the MB solution and stirred in the dark for 2 h to achieve adsorption-desorption equilibrium between dye and photocatalyst. The reaction mixture was exposed to sunlight for 4 h (11 am to 3 pm). The sample was withdrawn every 1 h and centrifuged to separate the catalyst from the sample aliquot. The after-reaction concentration of MB was determined by measuring the absorbance of the supernatant at 664 nm using a UV-Vis spectrophotometer. The MB removal percentage ( $\frac{C_t}{C_0} \times 100$ ) is plotted against the time taken for the degradation with respect to Beer-Lambert's Law. The  $C_0$  is the initial MB concentration whereas  $C_t$  is the MB concentration after a certain period of irradiation [29]. The effect of photocatalyst dosage, pH, Bi concentration, and MB concentration was evaluated to obtain the optimum photodegradation conditions. The

reusability of the photocatalyst has also been tested under the optimum reaction conditions.

The Langmuir–Hinshelwood (LH) kinetics is a widely used kinetic model for the photodegradation of organic contaminants in solution [30–32]. The dependent rate of photodegradation on their concentration can be expressed as:

$$\frac{1}{r} = \frac{1}{k_r} + \frac{1}{k_r k_f C} = \frac{k_f C}{1} + KC \quad \text{Equation 1}$$

where  $r$  is the reaction rate for the oxidation of the reactant,  $k_r$  is the specific reaction rate constant for the oxidation of the reactant,  $k_a$  is the equilibrium constant of the reactant, and  $C$  is the dye concentration. The equation can be simplified to a first-order equation when the concentration is very low ( $C_0$  is small).

$$-\ln\left(\frac{C_0}{C_t}\right) = kt \quad \text{Equation 2}$$

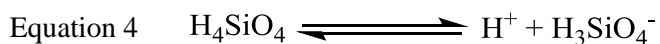
### 3. Results and Discussion

#### 3.1 Characterisation of the photocatalysts

##### 3.1.1 Scanning electron microscopy/energy dispersive X-ray (SEM/EDX) Analysis

The concentration of bismuth detected by EDX analysis on the surface of the photocatalysts is shown in **Table 1**. The SEM analysis indicates that the surface of RHS (**Fig. 1(a)**) is porous with some agglomerated particles. The average diameter of the pore opening was measured to be 1.13  $\mu\text{m}$ . The porous nature of the RHS is attributed to the rinsing process using hot water. Amorphous silica is soluble in hot water depending on the concentration of other dissolved species, such as NaCl. Each of the four oxygen atoms surrounding every silicon atom is connected to another silicon atom. The components can dissolve when in contact with hot water to form silicic acid,  $\text{H}_4\text{SiO}_4$ , as shown in Equation 3. Silicic acid is a weak acid that can undergo partial dissociation to form  $\text{H}_3\text{SiO}_4^-$  (Equation 4), which is

soluble in water [18]. The uneven dissolution of silica layers may have created the pores.



The surface of RHSBi-A1, RHSBi-A2, and RHSBi-A3 (**Fig. 1(b)-(d)**) was observed to have a smaller average pore diameter compared to RHS. The average diameter of the pores opening was measured to be 0.84  $\mu\text{m}$ , 0.78  $\mu\text{m}$ , and 0.72  $\mu\text{m}$ , respectively. Compared to the silicate layer, the bismuth-silicate layer cannot or weakly dissolve in the hot water. Hence, the pores could be formed on the areas that did not contain a bismuth-silicate layer. The number of pores observed on the surface of RHSBi-A4 is lesser compared to the rest of the photocatalysts due to the formation of the higher degree of bismuth-silicate layer. Also, during rinsing, the physically adsorbed  $\text{Bi}_2\text{O}_3$  can be removed, hence creating pores. The chemically bonded small-sized  $\text{Bi}_2\text{O}_3$  could reside within the silica framework. The pore-creation process is simplified in **Scheme 1**.

##### 3.1.2 X-Ray diffraction (XRD) Analysis

The crystallinity of RHS and RHSBi photocatalysts was determined using the XRD analysis, and their diffractograms are depicted in **Fig. 2(a)**. Only a single broad peak at  $2\theta = 22\text{--}23^\circ$  which is attributed to amorphous silica can be seen in the diffractograms [34]. XRD diffraction peaks related to  $\text{Bi}_2\text{O}_3$  was not observed in the diffractogram since the physically adsorbed  $\text{Bi}_2\text{O}_3$  nanoparticles have been removed during rinsing with hot water. The smaller-sized  $\text{Bi}_2\text{O}_3$  nanoparticles that were chemically integrated into the silica matrix may have escaped detection during analysis since crystallites with less than 10 nm are more likely to produce diffraction lines with low intensity, thus, making them indistinguishable from the noise [35].

**Table 1.** Bi content and porosity of RHS and RHSBi photocatalysts.

Catalyst	Bi Content (wt%)	Specific Surface Area, $S_{\text{BET}}$ ( $\text{m}^2/\text{g}$ )	Pore Size, $d_p$ ( $\text{\AA}$ )	Total Pore Volume, $V_p$ ( $\text{cm}^3/\text{g}$ )
RHS	0	19.1	516	0.14
RHSBi-A1	3	30.5	554	0.26
RHSBi-A2	4	6.3	297	0.02
RHSBi-A3	7	5.6	304	0.02
RHSBi-A4	10	15.8	408	0.09

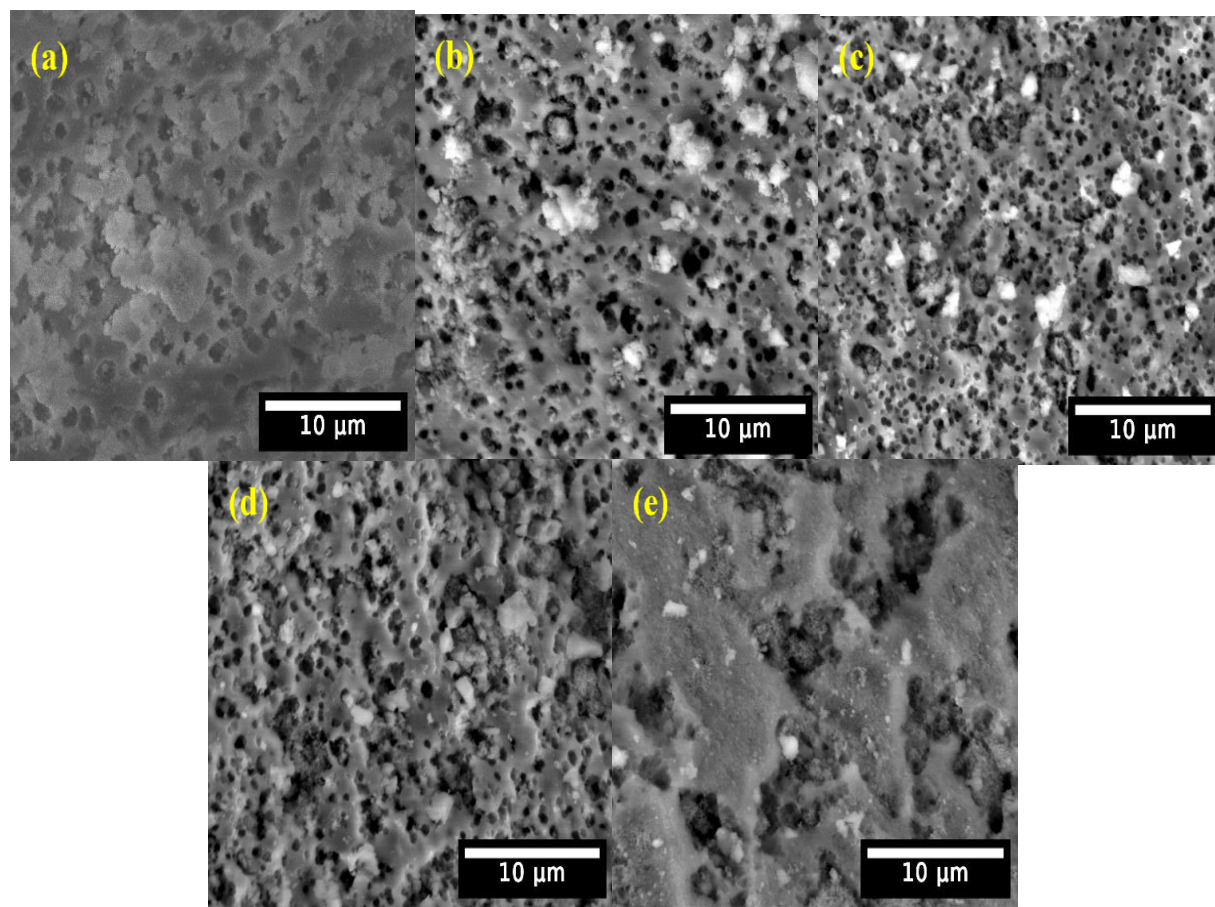
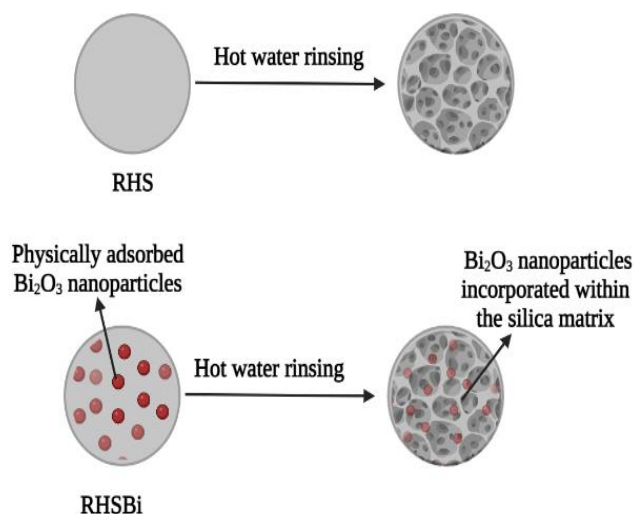


**Fig. 1.** The SEM micrographs of (a) RHS, (b) RHSBi-A1, (c) RHSBi-A2 (d) RHSBi-A3 and (e) RHSBi-A4.



**Scheme 1.** Rinsing the RHS and RHSBi photocatalyst with hot water dissolves the silica layer and also removes physically adsorbed  $\text{Bi}_2\text{O}_3$  nanoparticles.

### 3.1.3 Fourier-transform infrared (FTIR) Analysis

The FTIR spectra of the RHS and RHSBi photocatalysts are shown in **Fig. 2(b)**. The IR peak in the 3000-3800

$\text{cm}^{-1}$  range is a characteristic of -OH stretching vibration of the silanol (Si-OH), metal-O modes, and adsorbed water molecules [36-37]. The IR peak around  $1650 \text{ cm}^{-1}$  is a characteristic of H-O-H bending vibration [38]. The characteristic peaks of asymmetric stretching vibration, symmetric stretching vibration, and bending vibration of the Si-O-Si bond can be found at  $1080 \text{ cm}^{-1}$ ,  $794 \text{ cm}^{-1}$ , and  $452 \text{ cm}^{-1}$ , respectively. The  $400\text{-}700 \text{ cm}^{-1}$  peaks could also be attributed to the Bi-O bond in the RHSBi photocatalysts [39].

### 3.1.4 $\text{N}_2$ adsorption-desorption Analysis

The  $\text{N}_2$  adsorption-desorption isotherms (**Fig. S1**) of RHS and RHSBi photocatalysts exhibit Type IV isotherm according to the classification of International Union of Pure and Applied Chemistry (IUPAC), which is typical for mesoporous solids with pore size distribution in the range of 20-500 Å. The hysteresis loop observed is classified as H2(b) under the IUPAC classification. The H2(b) hysteresis loop indicates that the synthesised solids have a complex ink-bottle-shaped pore system consisting of narrow pore bodies with a wide neck size distribution [40].

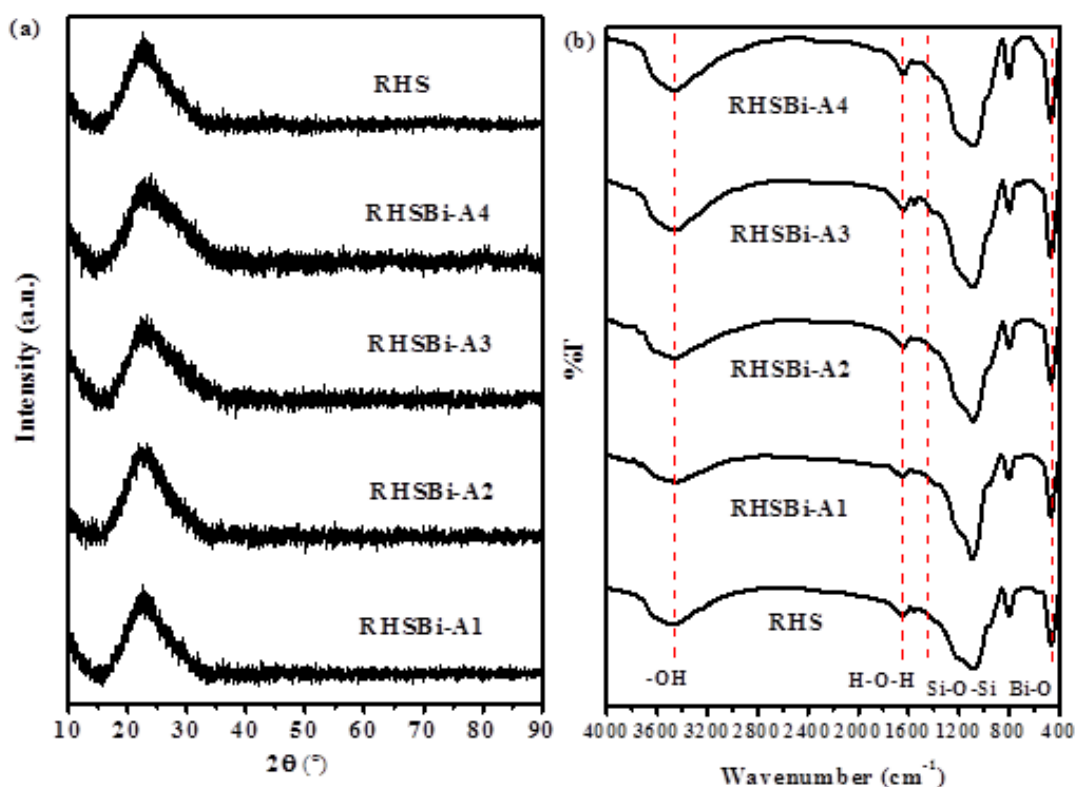


**Fig. 2.** (a) XRD diffractogram and (b) FTIR spectrum of RHS and RHSBi photocatalysts.

The Barrett, Joyner, and Halenda (BJH) pore size distribution ( $d_p$ ), specific Brunauer-Emmett-Teller surface area ( $S_{BET}$ ), and pore volume are given in **Table 1**. The higher  $S_{BET}$ ,  $d_p$  and  $V_p$  of RHSBi-A2 could be attributed to its higher porosity. Further increase in the bismuth content resulted in pore clogging and the formation of more bismuth-silicate layers leading to a drop in  $S_{BET}$ ,  $d_p$ , and  $V_p$ . The pore size distribution curves are given in **Fig. S2**. The pore size measurement done using SEM analysis contradicts the  $N_2$  adsorption-desorption analysis. In general, highly porous solids will have greater  $S_{BET}$ . The difference is that the SEM only indicates the pores on the surface, whereas  $N_2$  gas can penetrate deeper into the solids and provide comprehensive pore size and surface area analysis.

### 3.1.5 UV-Visible spectrophotometry diffuse reflectance spectroscopy (UV-Vis DRS)

The RHSBi photocatalysts' indicate a strong UV band centered around 235 nm (**Fig. 3(a)**), implying a ligand-to-metal charge transfer involving isolated Bi atoms (Si-O-Bi-O-Si) sites, which may be in tetrahedral coordination in the silica network [41,42]. The intensity of this peak is noticed to increase with the concentration

of bismuth. This is expected since more Bi-active sites are available for UV absorption. The band edge was noticed to be shifted to the visible region. This indicates that the RHSBi photocatalysts is effective in utilising visible light.

The bandgap energy was estimated using Tauc's equation, shown in Equation 5.

$$\alpha h\nu = A(h\nu - E_g)^{1/n} \quad \text{Equation 5}$$

$\alpha$  is the absorption coefficient,  $h$  is Planck's constant,  $\nu$  is the light frequency,  $A$  is the proportionality constant, and  $E_g$  is the bandgap energy. Mehrabanpour et al. have summarised several Tauc's plot that has been reported in the literature [43]. The equations are given in **Table 2**. The value of  $n$  is specific depending on the type of electronic transition (indirect forbidden (IF), indirect allowed (IA), direct forbidden (DF), and direct allowed (DA) transitions).

The bandgap energy of the RHSBi photocatalysts was estimated from a Tauc plot of  $(\alpha h\nu)^n$  versus  $h\nu$  (**Fig. 3(b)**). The estimated bandgap by extrapolating of the rising slope of the curves toward the x-axis, was around 3.77-3.79 eV.

**Table 2.** The list of Tauc's equation.

Equation	n value				Ref.
	IF	IA	DF	DA	
$F(R) h\nu = A (h\nu - E_g)^n$	3	3	3/2	1/2	[44]
$(F(R) h\nu)^n = A (h\nu - E_g)$	1/3	1/2	2/3	2	[45]
$(\alpha h\nu)^{1/n} = A (h\nu - E_g)$	3	2	3/2	1/3	[46]
$(\alpha h\nu) = A (h\nu - E_g)^{1/n}$	1/3	1/2	2/3	2	[47]
$(\alpha h\nu) = A (h\nu - E_g)^{n/2}$	6	4	3	1	[48]
$(\alpha h\nu)^{2/n} = A (h\nu - E_g)$	6	4	3	1	[48]

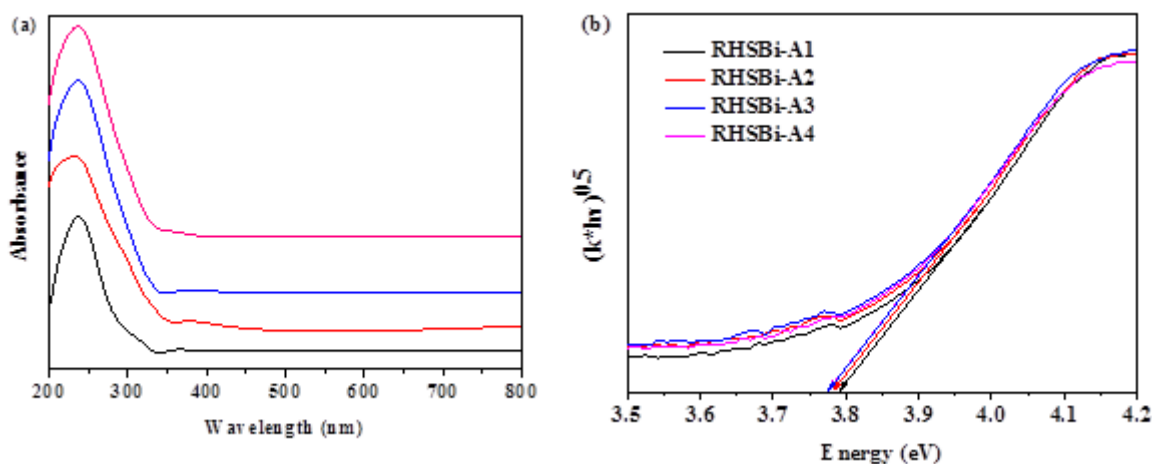


**Fig. 3.** (a) UV-Vis DRS spectra and (b) Tauc plot of  $(\alpha h\nu)^{0.5}$  versus  $h\nu$  of RHS and RHSBi photocatalysts. The band gap was estimated around 3.77-3.79 eV.

### 3.1.6 Raman Spectroscopy Analysis

The chemical environment of RHSBi photocatalysts was further analysed using Raman spectroscopy. As shown in **Fig. S3(a)-(d)**, four signals emerged in the Raman spectra. A strong and highly polarised band at  $\sim 200 \text{ cm}^{-1}$  was attributed to  $\text{Bi}^{3+}\text{-O}$  vibrations [49]. The intensity of this peak increased with increasing Bi concentration, showing that  $\text{Bi}^{3+}$  cations were successfully introduced into the silica framework. The peak intensity decreased abruptly when the doping dosage increased to 10% due to the formation of barium silicate particles. An absorption band appeared at  $1100 \text{ cm}^{-1}$  due to the presence of asymmetric stretching Bi-O-Si configurations [30]. This peak continues to intensify with increasing Bi doping dosage. This is associated with the emergence of a Bi-O vibration peak at  $600 \text{ cm}^{-1}$  that shows the elongation of clusters [50].

### 3.1.7 Determination of pH of point of zero charge ( $\text{pH}_{\text{PZC}}$ )

The pH of the point of zero charge ( $\text{pH}_{\text{PZC}}$ ) is a pH at which the surface of a solid has an equal number of positive and negative charges; hence the surface charge becomes null and zero [32, 33]. Below the  $\text{pH}_{\text{PZC}}$  value, the surface of a solid has a native negative charge (basic)

feature which attracts the adsorption of a proton from the reaction solution. Thus, the net surface charge becomes positive. This positively charged environment favours the adsorption of anionic pollutants. Above the  $\text{pH}_{\text{PZC}}$  value, the native positive charge (acidic) feature will dominate, hence, attracting the adsorption of hydroxyl anions resulting in a negative surface charge. Thus, cationic pollutants will be attracted to the negatively charged surface [43,53]. The pollutants and the photocatalyst's surface must be oppositely charged for optimum removal of pollutants through photocatalysis or adsorption. The  $\text{pH}_{\text{PZC}}$  of RHSBi photocatalysts was determined to be around pH 8.1. The plot of  $\Delta\text{pH}$  vs.  $\text{pH}_i$  for the PZC determination is shown in **Fig S4**.

## 3.2 Photocatalytic degradation test

### 3.2.1 Effect of the pH

The effect of the pH on the photocatalytic removal of MB was investigated using RHSBi-A4 at pH 5, 8, and 10. The mixture was stirred in the dark for 2 h to achieve adsorption-desorption equilibrium. The removal profile diagram is shown in **Fig. 4(a)**. From the profile, the adsorption was highest at pH 10 (25%) and lowest at pH 5 (3%). This observation is attributed to the electrostatic

attraction between the MB and the photocatalysts. The  $pH_{PZC}$  of the RHSBi photocatalysts was determined to be around 8.1. When the pH of the solution is pH 5, the surface of the photocatalysts will be positively charged, similar to the charge of MB; hence, electrostatic repulsion will dominate. When the solution pH was increased to more than the  $pH_{PZC}$  value, the surface of the photocatalyst became negatively charged and attracted cationic MB.

For the photocatalytic process to take place, pollutants have to be adsorbed on the surface of the photocatalyst. Lower adsorption will yield lower degradation during the photocatalysis process. Whereas, if the adsorption is too strong or thick adsorption layers, photons will not be able to be effectively absorbed for the generation of radicals. The removal of MB continued to be removed at pH 10 under sunlight irradiation up to 49.5% whereas due to lack of adsorption at pH 5, only 28% of MB was removed [55]. Menting et al, reported that an increased in photocatalytic removal at alkaline pH facilitates is also contributed by the production of hydroxyl radical ( $OH\cdot$ ) from the reaction between  $h^+$  and  $OH^-$  [56]. The remaining reaction parameters were evaluated at pH 10 due to better photocatalytic removal.

### 3.2.2 Effect of bismuth concentration

The effect of bismuth concentration, photolysis, and adsorption on the removal of MB is shown in **Fig. 4(b)**. The removal of MB without any photocatalysts was determined to be less than 10% and the adsorption reached equilibrium at 2 h. The rate of adsorption for RHS, RHBi-A1 RHBi-A2, RHBi-A3, and RHBi-A4 was 81.9%, 57.1%, 80.1%, 63.4%, and 64.6%, respectively. The adsorbed MB on the surface of RHS was noticed to be desorbed after 2 h due to the weak electrostatic attraction between the MB molecules and the surface of the photocatalyst.

The higher adsorption capacity of the photocatalysts is attributed to the electrostatic attraction between the photocatalyst surface and the MB and also the highly porous surface. Among the photocatalysts, the RHSBi-A2 achieved the highest adsorption (81%) due to its smallest pore size distribution which caused the diffused MB molecules to be trapped inside the pores and unable to diffuse out. Exposure to the sun, improved the removal around 3%. Lower MB removal due to photocatalysis is attributed to the saturation of the photocatalyst surface with the MB molecules, which prevented the light from reaching the surface to create electron-hole pairs to induce the photocatalysis process.

Regardless, the study was continued using RHSBi-A2 based on its highest removal.

### 3.2.3 Effect of MB initial concentration

The effect of MB initial concentration on the photocatalytic properties of RHSBi-A2 is depicted in **Fig. 4(c)**. As the initial MB concentration increased, the adsorption was observed to decrease. The decrease is attributed to the lack of available active sites for adsorption and due to mass transfer limitation [57–59]. The contribution from photocatalysis was observed to be less. When the adsorption layer became thick, less light will reach the surface of the photocatalyst for photon absorption. As a result, less radical will be generated for photodegradation [56]. The highest total MB removal was at 10 ppm (90%) whereas the lowest removal was at 25 ppm (14.5%). Subsequent parameter optimisation was carried out using an initial MB concentration of 10 ppm.

### 3.2.4 Effect of photocatalyst dosage

The effect of photocatalyst dosage on the removal of MB is shown in **Fig. 4(d)**. The adsorption of MB increased as the dosage was increased from 25 mg to 50 mg due to the increasing availability of the active sites, and the removal of MB continued to increase when exposed to sunlight. However, a further increase in the dosage of catalysts to 75 mg, decreased the adsorption and photodegradation of MB. The highest MB removal (90%) was achieved when 50 mg of RHSBi-A2 was used. Excessive dosage (75 mg in this work) caused the photocatalyst to agglomerate forming bigger aggregates. In larger aggregates, most of the internal volume cannot be excited by light due to scattering. As a result, its light absorption and quantum efficiency will be lower [60]. The lack of light will prevent the formation of photogenerated electron/hole pairs needed for effective photocatalytic removal [61], [62]. The collision between excited or activated photocatalyst with ground state photocatalyst will deactivate them and suppress the formation of  $e^-/h^+$  pairs as well. Hence, the optimum dosage was determined to be 50 mg. **Fig. 4(f)** shows the plots of  $\ln(C_0/C_t)$  versus time of the photocatalysts. All the  $R^2$  values were corrected using non-linear fitting. A good linear relation between  $\ln(C_0/C_t)$  versus time indicates that the photodegradation of MB using these photocatalysts obeys the rules of the LH kinetic model and the first-order reaction kinetics. RHSBi-A2 is selectively chosen to represent the rate equation because it has the highest photodegradation efficiency (86.5%) at optimum pH and dosage compared to the other photocatalysts.

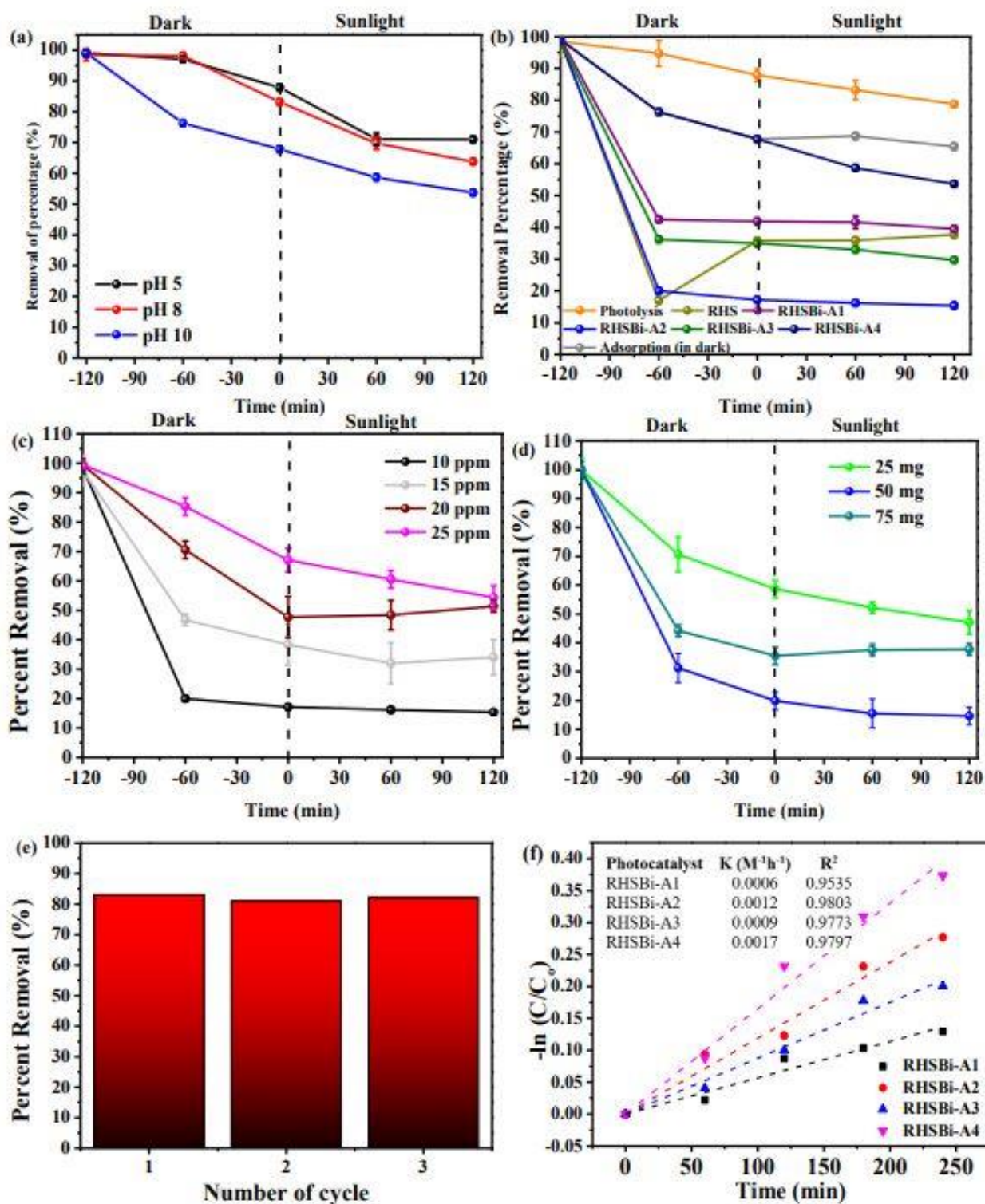


**Fig. 4**(a) Effect of pH on the MB removal by RSHBi-A4 (photocatalyst dosage: 50 mg, MB concentration: 10 ppm: volume of MB solution: 200 mL, reaction time: 4 h), (b) Effect of bismuth concentration on the MB removal (photocatalyst dosage: 50 mg, MB concentration: 10 ppm: volume of MB solution: 200 mL, reaction time: 4 h), (c) Effect of initial MB concentration (photocatalyst dosage: 50 mg RSHBi-A2: volume of MB solution: 200 mL, reaction time: 4 h), (d) Effect of RSHBi-A2 dosage on the MB removal (MB concentration: 10 ppm: volume of MB solution: 200 mL, reaction time: 4 h), (e) reusability of RSHBi-A2 under the optimum conditions (dosage: 50 mg, MB concentration: 10 ppm, volume of MB solution: 200 mL, reaction time: 4 h) and (f) Langmuir-Hinshelwood pseudo-first-order MB photodegradation kinetics fitting.

### 3.2.6 Possible photocatalytic degradation mechanism

Photodegradation mechanism of MB using the RHSBi-A2 is proposed based on the Valence Band ( $E_{VB}$ ) and Conductive Band ( $E_{CB}$ ) potentials using Mulliken Theory (Equations 6 and 7). The Mulliken symbol ( $\chi$ ) is determined using Equation 8.

$$E_{CB} = \chi - 0.5E_g - E_c \quad \text{Equation 6}$$

$$E_{VB} = E_{CB} + E_g \quad \text{Equation 7}$$

$$\chi = [(A)^a (B) (C)]^{1/a+b+c} \quad \text{Equation 8}$$

where  $E_g$  is the band gap potential and  $E_c$  is the energy of free electrons vs. hydrogen (4.5 eV). The  $\chi$  is the Mulliken (Absolute) electronegativity: A, B, and C are the distinct species in the semiconductor: a, b, and c are the number of atoms of the distinct species. The value of  $E_g$  determined by UV-Vis reflectance is 3.79 eV. The  $E_{CB}$  and  $E_{VB}$  of RHSBi-A2 are estimated to be -2.42 eV and 1.37 eV, respectively.

When light was absorbed, electrons will be excited from the valence band (VB) to the conduction band (CB), leaving behind holes in the VB ( $h_{VB}^+$ ) (Equation 7). Since the  $E_{CB}$  potential is more negative than that of  $O_2/\cdot O_2^-$  (-0.33 eV), the photogenerated electrons in CB ( $e_{CB}^-$ ) can convert the adsorbed oxygen on the surface to  $O_2\cdot^-$  that could react with water to produce  $\cdot OH$  radicals [63, 64]. In addition, the  $e_{CB}^-$  can be transferred to the silica framework. In other words, the silica framework acts as electron reservoirs [65, 21]. Furthermore, the  $e_{CB}^-$  can also directly react with the MB to form reduction products. The  $E_{VB}$  is less positive than that of  $\cdot OH/H_2O$  (+2.27 eV) and  $\cdot OH/OH^-$  (+1.99 eV). Hence, the  $h_{VB}^+$  is

unable to convert  $H_2O$  or  $OH^-$  form  $\cdot OH$  [63]. However, the  $h_{VB}^+$  has intrinsic oxidation capacity which can directly react with the MB to form oxidised products [66–68]. The photocatalytic degradation mechanism is simplified in Fig. 5. The detailed MB photodegradation route and the intermediates formed has been widely reported in the literature. In addition to the organic components, inorganic components such as chloride, nitrate, and sulfate anions was also detected [69, 70].

### 3.2.5 Reusability Study

The reusability of RHSBi-A2 for the photocatalytic degradation of MB under the optimum conditions (dosage: 50 mg, MB concentration: 10 ppm, volume of MB solution: 200 mL, Reaction time: 4 h) is shown in Fig. 4(e). The result showed that RHSBi-A2 is very stable and only experienced a slight decrease to 89% after three cycles of photodegradation reaction.

### 3.2.7 Comparison Study with other reported photocatalysts

The ability of RHSBi-A2 in photocatalytic degrading MB was compared with several Bi-based photocatalysts reported in the literature. As shown in Table 3, RHSBi-A2 requires a longer time to reach similar MB removal. Even though sunlight is used as well in the reports, it can be very unpredictable, and the light intensity varies depending on the latitude and longitude. Furthermore, the lower surface area could also contribute to its lower removal efficiency. Artificial light, such as xenon and halogen lamps, is expected to give better results since they can give constant intensity.

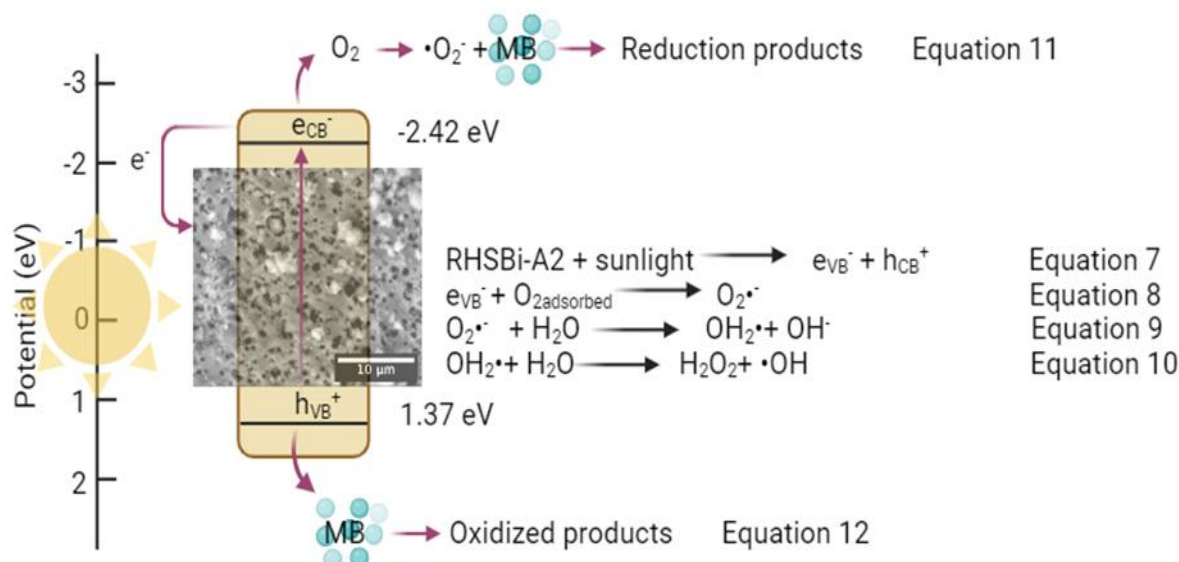


Fig. 5. The possible photocatalytic degradation mechanism of MB using RHSBi-A2 under sunlight irradiation.

**Table 3.** Comparison of photodegradation of methylene blue over the catalyst.

Catalyst	Reaction conditions	Light source	Degradation efficiency %	Radiation time	Ref.
15 wt.% Bi <sup>3+</sup> -doped CeO <sub>2</sub> nanoparticles	[MB] = 10 <sup>-5</sup> M Catalyst dosage = 1 mg/L	Halogen lamp (300 W)	100	75 min	[71]
5% Bi/4% Ti-MCM-41	[MB] = 4 x 10 <sup>-5</sup> M Catalyst dosage = 1000 mg/L	Xenon lamp (300 W)	100	<40 min	[20]
La <sub>0.85</sub> Bi <sub>0.15</sub> CoO <sub>3</sub>	[MB] = 10 mg/L Catalyst dosage = N/A	sunlight	98.5	80 min	[72]
Bi@SiNWs	[MB] = 10 <sup>-5</sup> M Catalyst dosage = 250 mg/L	sunlight	89	120 min	[73]
Gd <sub>0.5</sub> Bi <sub>0.5</sub> FeO <sub>3</sub>	[MB] = 5 mg/L Catalyst dosage = 1000 mg/L	Xenon lamp (500 W) with a 420 nm cutoff filter	82.1	180 min	[74]
BSC_NS250 silica-modified self-assembled structures of bismutite	[MB] = 5 mg/L Catalyst dosage = 250 mg/L	Xenon arc lamp (300 W)	92.6	60 min	[3]
10 wt.% mSiO <sub>2</sub> /BiVO <sub>4</sub>	[MB] = 10 mg/L Catalyst dosage = 50 mg	Visible light	90.8	60 min	[21]
RHSBi-A2	[MB] = 10 mg/L Catalyst dosage = 250 mg/L	Sunlight	90	240 min	Present work

#### 4. Conclusions

This study highlights the synthesis of amorphous mesoporous bismuth-silicate nanocomposite using rice husk ash (RHA) as silica precursor via the sol-gel method for the photocatalytic removal of MB under sunlight. The optimum MB degradation was achieved using 50 mg of RHSBi-A2 in 10 ppm of MB solution at pH 10. The photocatalytic reaction was found to fit the Langmuir–Hinshelwood pseudo-first-order model with a rate constant of 0.0012 M<sup>-1</sup>h<sup>-1</sup> (R<sup>2</sup>=0.9803). It was evidenced that the catalytic performance of RHSBi-A2 does not change significantly after three cycles of reaction. The improved performance of this photocatalyst, is attributed to its pore size which traps the MB molecules and subsequently promote photodegradation. The photocatalytic degradation of MB is proposed to be driven by the formation of superoxide radicals (O<sub>2</sub><sup>•-</sup>) hydroxyl radicals (•OH) and

holes (h<sup>+</sup>) based on the E<sub>VB</sub> and E<sub>CB</sub> of the photocatalyst. RHSBi-A2 required a longer time compared to the reported photocatalysts in the literature due to low surface area. The use of sunlight also contributed to the lower removal percentage since sunlight intensity can be very unpredictable.

#### Acknowledgements

This research was funded by the Ministry of Education Malaysia (Higher Education) for the Fundamental Research Grant Scheme (FRGS/1/2023/STG01/USM/02/2). Anwar Iqbal would like to thank National Research and Innovation Agency (BRIN), Government of Republic of Indonesia for the appointment as Visiting Researcher Fellowship (File No. B-4090/IL.5/SI/12/2022).

#### Declaration of Competing Interest

The authors declare no conflict of interest.

## Author Contributions

AI, NHH and DHYY.: conceptualisation, AI, NJ, and HJY: methodology, AI, NHH, NJ and HJY: formal analysis, AI, NHH, DHYY, NJ and HJY: investigation, AI, NHH and DHYY: resources, AI, NHH and DHYY: data duration, AI, NHH and DHYY: visualisation, AI, NHH, DHYY, NHMK, MNA and SM: writing—original draft, AI, NHH and DHYY: writing—review & editing, AI, NHH and DHYY: supervision. All authors reviewed the manuscript.

## References

- [1] H. Regen. Asian rivers are turning black. And our colorful closets are to blame (2020). doi: <https://edition.cnn.com/style/article/dyeing-pollution-fashion-intl-hnk-dst-sept/index.html>
- [2] R.A. Basit, Z. Abbasi, M. Hafeez, P. Ahmad, J. Khan, M.U. Khandaker, K.S. Al-Mugren, A. Khalid, Crystals. 13(2), 2023, 281.
- [3] J. Antony, S.V. Gonzalez, S. Bandyopadhyay, J. Yang, M. Rønning, Catal. Today. 413-415 (2023) 2113986.
- [4] The Bangladesh Responsible Sourcing Initiative: A new model for green growth. International Bank for Reconstruction and Development/ The World Bank (2014).doi:<https://documents.worldbank.org/en/publication/documentsreports/documentdetail/614901468768707543/the-bangladesh-responsible-sourcing-initiative-a-new-model-for-green-growth>.
- [5] N. Tahir, M. Zahid, I.A. Bhatti, Y. Jamil Y, Environ. Sci. Pollut. Res. 29 (2022) 6552–6567.
- [6] M.T. Yagub, T.K. Sen, S. Afroze, H.M. Ang, Adv. Colloid Interface Sci. 209 (2014) 172-184.
- [7] A. Makofane, D. E. Motaung, N. C. Hintsho-Mbita, Ceram. Int. 47(16) (2021) 22615–22626.
- [8] T. de Oliveira Guidolin *et al.*, J. Clean. Prod. 318 (2021) 128556.
- [9] T.Q.Q. Viet, V.H. Khoi, N.T.H Giang, H.T.V Anh, N.M. Dat, M.T. Phong, N.H. Hieu, Colloids Surf. A: Physicochem. Eng. Asp. 629 (2021) 127464.
- [10] Z. Zahid, A. Rauf, M. Javed, A. Alhujaily, S. Iqbal, A. Amjad, M. Arif, S. Hussain, A. Bahadur, N.S. Awwad, H.A. Ibrahim, F.F. Al-Fawzan, E.B. Elkaeed, Inorganics. 11(3) (2023) 133.
- [11] D. Chahar, D. Kumar, P. Thakur, A. Thakur, Mater. Res. Bull. 62 (2023) 112205.
- [12] M. Golmohammadi, H. Hanafi-Bojd, M. Shiva, Ceram. Int., 49(5) (2023) 7717–7726.
- [13] L. Wang, X. Wang, J. Yin, Y. Zhu, C. Wang, Catal. Commun. 87 (2016) 98-101.
- [14] T. Seyedi-Chokanlou, S. Aghabeygi, N. Molahasani, F. Abrinaei, Iran. J. Catal., 11(1) (2021) 49–58.
- [15] D. Nunes, A. Pimentel, R. Branquinho, E. Fortunato, R. Martins, Catalysts, 11(4) (2021) 504.
- [16] A. Singh, A. K. Singh, J. Liu, and A. Kumar, Catal. Sci. Technol., 11(12) (2021) 3946–3989.
- [17] M. Stetsenko *et al.*, Antireflection enhancement by composite nanoporous zeolite 3A–carbon thin film, Nanomaterials, 9(1) (2019) 1641
- [18] P. Aggrey *et al.*, Opt. Mater., 133 (2022) 113048
- [19] Y.A. Belik, A.A. Vodyankin, E.D Fakhruddinova, V.A. Svetlichnyi, O.V.J Vodyankina, J. Photochem. Photobiol. A: Chem. 195 (2022) 174-183.
- [20] S.K. Mohamed, A.A. Ibrahim, A.A. Mousa, M.A. Betiha, E.A. El-Sharkawy, H.M.A Hassan, Sep. Purif. Technol.195 (2018) 174-183.
- [21] A.S. El-Hakam, F.T. ALShorifi, R.S. Salama, S. Gamal, W.S.A. El-Yazeed, A.A. Ibrahim, I.A. Ahmed J. Mater. Res. Technol. 18 (2022) 1963-1976.
- [22] I. J. Fernandes *et al.*, Mat. Res., 20(2) (2017) 512–518.
- [23] R. Haus, S. PRinz, and C. Priess, Assessment of High Purity Quartz Resources. Berlin Heidelberg: Springer, 2012.
- [24] J. N. Appaturi, F. Adam, Appl. Catal. B. 136–137 (2013) 150–159.
- [25] N. H. Ibrahim, A. Iqbal, N. Mohammad-Noor, M. R. Roziawati, S. Sreekantan, A. S. Zulkipli, 57 (2022) 1184–1190.
- [26] F. Adam, A. Iqbal, Chem. Eng. J. 171(3) (2011) 1379–1386.
- [27] S. Y. Yao, A. Iqbal, N. H. H. Abu Bakar, M. R. Yusop, H. Pauzi, D. Kanakaraju, ChemistrySelect, 7(40) (2022) e202201970.
- [28] B. Divband, A. Jodaie, M. Khatmian, Iran. J. Catal., 9(1) 63–70.
- [29] L. Kratofil Krehula *et al.*, Polym. Bull., 76(4) (2019) 1697–1715.
- [30] Z. Pan, D. O. Henderson, S. H. Morgan, J Non Cryst Solids, 171(2) (1994) 34–140.
- [31] W. Zhang, Y. Li, C. Wang, and P. Wang, Desalination, 266 (1-3) (2011) 40–45.

- [32] Z.-D. Meng et al., *Mater. Sci. Eng. C*, 32(8) (2012) 2175–2182.
- [33] K. Brown, *Thermodynamics and kinetics of silica scaling. International Workshop on Mineral Scaling*. 2011.
- [34] G. Nallathambi, T. Ramachandran, V. Rajendran, R. Palanivelu, *Mat. Res.* 14 (4) (2011) 554-559.
- [35] C.F. Holder, R.E. Schaak, *ACS Nano*. 13(7) (2019) 7359–7365.
- [36] S. Aprilia, C.M. Rosnelly, Zuhra, F. Fitriani, E.H. Akbar, M. Raqib, K. Rahmah, A. Amin, R.A. Baity, S. *Mater. Today: Proc.* 87 (2023) 225-229.
- [37] I. Rashid, N. Daraghme, M. Al-Remawi, S.A. Leharne, B.Z. Chowdhry, A. Badwan, *J. Pharm. Sci.* 98 (2009) 4887-4901
- [38] S. Sankar, N. Kaur, S. Lee, D.Y. Kim, *Ceram. Int.* 44 (2018) 8720-8724
- [39] Y. Astuti, A. Fauziyah, S. Nurhayati, A.D. Wulansari, R. Andianingrum, A.R. Hakim, G. Bhaduri. *IOP Conf. Ser.: Mater Sci Eng.* 107 (2016) 012006.
- [40] K.A. Cychosz, M. Thommes, *Engineering*. 4(4) (2018) 559-566.
- [41] R. Kumar, N. Enjamuri, J.K. Pandey, D. Sen, S. Mazumder, A. Bhaumik, B. Chowdhury. *Appl. Catal. A: Gen.* 497 (2015) 51-57.
- [42] A.K.R. Police, S. Basavaraju, D.K. Valluri, S. Machiraju, *J. Mater. Sci. Technol.* 29 (2013) 639-646.
- [43] N. Mehrabanpour, A. Nezamzadeh-Ejhieh, S. Ghattavi, A. Ershadi, *Appl. Surf. Sci.*, 614 (2023) 156252.
- [44] H. Che, G. Che, E. Jiang, C. Liu, H. Dong, C. Li, *J Taiwan Inst Chem Eng*, 91 (2018) 224–234.
- [45] P. Norouzzadeh, Kh. Mabhouti, M. M. Golzan, R. Naderali, *Optik*, 204 (2020) 164227.
- [46] P. Makuła, M. Pacia, W. Macyk, *J. Phys. Chem. Lett.*, 9(23) (2018) 6814–6817.
- [47] R. Köferstein, L. Jäger, S. G. Ebbinghaus, *Solid State Ionics*, 249–250 (2013) 1–5
- [48] K. Katsumata, R. Motoyoshi, N. Matsushita, K. Okada, *J. Hazard. Mater.*, 260 (2013) 475–482.
- [49] A.J. Ward, A.M. Rich, A.F. Masters, T. Maschmeyer, *New J. Chem.* 37 (2013) 593-600.
- [50] Z. Lazarević, S. Kostić, V. Radojević, M. Romčević, M. Gilić, M. Petrović-Damjanović, Romčevićet, *N. Phys. Scr.* T157 (2013) 014046.
- [51] E.A. Al-Maliky, H.A. Gzar, M.G. Al-Azawy, *IOP Conf. Ser.: Mater. Sci. En.* 1184 (2021) 012004.
- [52] M. Kosmulski, *J. Colloid Interface Sci.* 1 (2011) 1-15.
- [53] S. Vahabirad, A. Nezamzadeh-Ejhieh, *Ecotoxicol. Environ. Saf.*, 263 (2023) 115254.
- [54] Z. A. AlOthman, M. A. Habila, R. Ali, A. Abdel Ghafar, M. S. El-din Hassouna, *Arab. J. Chem.*, 7(6) (2014) 1148–1158.
- [55] C. Yang et al., *Sci Rep*, 7(1) (2017) 3973.
- [56] Z. Mengting et al., *Environ. Pollut.*, 255 (2019) 113182.
- [57] D. Pathania, S. Sharma, P. Singh, *Arab. J. Chem.*, 10 (2017) S1445–S1451.
- [58] N. Barka, S. Qourzal, A. Assabbane, A. Nounah, Y. Ait-Ichou, *J. Saudi Chem. Soc.*, 15 (3) (2011) 263–267.
- [59] J. Iqbal et al., *Arab. J. Chem.*, 4(4) (2011) 389–395.
- [60] A. Tolosana-Moranchel, C. Pecharromán, M. Faraldos, A. Bahamonde, *Chem. Eng. Sci.*, 403 (2021) 126186.
- [61] D. Chen et al., *J. Clean. Prod.*, 268 (2020) 121725.
- [62] S. Ghanei-Zare, M. Moghadasi, R. Khajavian, N. Akbarzadeh-T, M. Mirzaei, *J. Mol. Struct.* (2023) 1286 135563.
- [63] F. Zheng et al., *J. Rare Earths*, 41(4) (2023) 539–549.
- [64] M. J. Kadhim, M. A. Mahdi, A. M. Selman, S. K. Jamel AlAni, J. J. Hassan, N. M. Ahmed, *Iran. J. Catal.*, 13(1) (2023)1-21
- [65] B. Naik, B. Nanda, K. K. Das, K. Parida, *J. Environ. Chem. Eng.* 5(5) (2017) 4524–4530
- [66] R. Ahmad, Z. Ahmad, A. U. Khan, N. R. Mastoi, M. Aslam, J. Kim, *J. Environ. Chem. Eng.*, 4(4) (2016) 4143–4164.
- [67] T. Senasu, S. Youngme, K. Hemavibool, S. Nanan, *J Solid State Chem* 297 (2021) 122088.
- [68] M. Yaghoubi-berijani, Ba. Bahramian, S. Zargari, *Iran. J. Catal.*, 10 (4) (2020) 307–317.
- [69] A. Nezamzadeh-Ejhieh, M. Karimi-Shamsabadi, *Appl Catal A-Gen*, 477 (2014) 83–92.
- [70] G. K. Parshetti, A. A. Telke, D. C. Kalyani, S. P. Govindwar, *J. Hazard. Mater.*, 176(1–3) (2010) 03–509.

[71] S. N. Veedu, S. Jose, S. B. Narendranath, M. R. Prathapachandra Kurup, P. Periyat, *Environ Sci Pollut Res*, 28(4) (2021) 4147–4155.

[72] K. Sathiyamoorthy, A. Silambarasan, S. Bharathkumar, J. Archana, M. Navaneethan, S. Harish, *Mater. Res., Bull.* 158 (2023) 112030.

[73] M. Naffeti, M.A. Zaïbi, C. Nefzi, A.V. García-Arias, R. Chtourou, P.A. Postigo, *Environ. Technol. Innov.* 30 (2023) 103133.

[74] Y. Ma, H. Shen, Y. Fang, H. Geng, Y. Zhao, Y. Li, J. Xu, Y. Ma, *Magnetochemistry*. 9 (2023) 45.